Plastic film residues on cropland: monitoring soil contamination through optical remote sensing

Alessandro Fabrizi [1], Peter Fiener [1], Kristof Van Oost [2], Florian Wilken [1]

[1] Institute of Geography, University of Augsburg, Augsburg, Germany
[2] Earth and Life Institute, Université Catholique de Louvain, Louvain-la-Neuve, Belgium

Correspondence to: Florian Wilken (florian.wilken@uni-a.de)

Abstract. Plastic films have been improving agricultural production and covering an increasing surface area of cropland in the last decades. Yet their use has been connected to the generation of plastic residues, potentially acting as a main secondary microplastic source in agricultural soils. Monitoring the generation of plastic film residues is crucial for identifying good management practices and assessing the risk of plastic use in agriculture. Remote sensing has been qualified as a valuable tool for monitoring macroplastic residues mainly on waters, while its use on agricultural soils is mostly unexplored. Our study combined proximal and remote sensing techniques to lay the foundations of UAV (Unmanned Aerial Vehicle) use for monitoring macroplastic film residues on cropland.

Through proximal and UAV acquisitions of five-bands multispectral data (i.e., blue, green, red, red edge, near infrared), we highlighted the potential of off-the-shelf miniaturised sensors and identified possible workflows for detecting macroplastic film residues. Our findings highlight a greater, or at least similar, efficacy of spatial resolution compared to spectral resolution, encouraging the use of high-resolution RGB cameras over multispectral cameras. Through proximal acquisitions of hyperspectral data on 8 different agricultural plastic films, we built spectral libraries and located absorption features at wavelengths that are not commonly available on off-the-shelf multispectral cameras. We highlighted that these absorption features unambiguously identify plastic films on cropland and offer the potential to distinguish plastic types, encouraging the development of sensors tailored for plastic detection.

1. Introduction

Soils are estimated to be a greater plastic sink than the ocean surface (Kedzierski et al., 2023; Lofty et al., 2022) and to potentially act as a plastic source for other environmental matrices through water and wind erosion (Rehm et al., 2021; Rezaei et al., 2022). In experimental setups high to very high concentrations of plastic have been shown to degrade soil physicochemical properties and affect plant health (Zhang et al., 2022), but the threshold concentrations at which these effects occur are still poorly quantified. Most likely, the source and physiochemical

properties of the plastic are important drivers (Wang et al., 2023b; Wang et al., 2023a; Liu et al., 2023), highlighting the necessity of tracing the origin of plastic contamination. The knowledge about the effects of current plastic contamination is still limited (Landrigan et al., 2023), while the ubiquitous presence, persistence, bioaccumulation, and possible unknown effects of plastic threaten soil health and call for plastic contamination monitoring plans.

Plastic in soil may span a wide range of polymers, shapes, sizes, and sources. One of the major sources and sinks of plastic are agricultural soils (Horton et al., 2017; Kawecki and Nowack, 2019), since plastic is extensively used in various ways to enhance productivity such as mulching and greenhouse films, or seed and fertiliser coatings (Fao, 2021; Eip-Agri Focus Group, 2021). Around 80 % of plastic use in European vegetable production is attributed to plastic films used as crop covers (Agriculture Plastic Environment Europe, 2019). While plastic films have been associated with the generation of macro- and microplastic residues (Steinmetz et al., 2022) (> 5 mm and < 5 mm, respectively (Thompson et al., 2004; Frias and Nash, 2019)) , their use can increase crop production and reduce the use of water and agrochemicals (Lamont, 2017; Espí et al., 2006). Mulching films can reduce evaporation from the soil surface and hence reduce the demand for water in dry regions or increase soil temperature in cold regions to improve the control of harvesting time. Additionally, mulching films can reduce weed growth and can be used for soil disinfestation to reduce the use of agrochemicals. Greenhouse films typically create a controlled environment for the growth of fruits and vegetables outside of typical growing seasons. Quantifying the residues generated after plastic film use and establishing monitoring tools is fundamental not only for assessing the environmental risk of plastic contamination, but also for identifying good management practices, aiming at a sustainable use of plastic films.

Plastic covers used in agriculture are mainly LDPE (low-density polyethylene) films with thickness ranging from 15 to 200 microns and lifetime ranging from a single cropping season to multiple years (e.g., 4 years) (Scarascia-Mugnozza et al., 2011). Thicker films are generally more resistant to mechanical stress and less likely to produce residues (Steinmetz et al., 2022). The usage beyond lifetime and other management practices, like application and removal modes, may also affect the amount of residues generated (Fao, 2021; Eip-Agri Focus Group, 2021).

Overall, earlier studies, such as the ones cited above, improved our understanding of plastic residue generation and concentration in soils but quantitative analyses are still hampered by the methodologies used for mapping plastic residues. Plastic is typically quantified by combining soil sampling and ex situ analyses, making comprehensive data collection and analysis on multiple fields slow. However, large-scale data collection is needed to cover the variety of plastic films used and management practices adopted.

The broad area coverage combined with very high spatial resolution offered by UAVs (Unmanned Aerial Vehicles) (Colomina and Molina, 2014) potentially enables data collection on multiple fields and detection of objects in the size range of macroplastic. UAV use has been explored to detect macroplastic on waters and

coastal areas first and foremost (Veenstra and Churnside, 2012; Martin et al., 2018), while applications on land are still limited.

Plastic materials are known to have unique absorption features in the SWIR (short wave infrared) (Kühn et al., 2004), and hyperspectral imaging has already been used for detecting floating macroplastic (Garaba and Dierssen, 2018). On land, the use of SWIR absorption features has been investigated for non-destructive microplastic detection (Pahlawan et al., 2025). Hyperspectral imaging has been used for the detection plastic covered surfaces (Zhou et al., 2021; Garaba, 2025; Despini et al., 2025) and pushed up to the identification of their functionality (e.g., greenhouses or photovoltaic panels) (Zhou et al., 2023). Bonifazi et al. (2023) have first shown the potential of using absorption features and hyperspectral imaging for the ex situ recognition of macroplastic residues found on agricultural soils. Still, reference spectral libraries are currently not available for agricultural plastics, and their establishment has been shown to push forward remote sensing algorithms for plastic detection (Garaba et al., 2018; Garaba et al., 2021). Despite the high potential of SWIR-based plastic detection, it must be considered that the absorption bands are typically available on hyperspectral sensors only, and their limited availability may hamper large-scale monitoring. Multispectral cameras offer a good compromise between data volume and spectral resolution, and the availability of off-the-shelf miniaturised sensors has favoured their use on low-payload UAVs. To the best of our knowledge, multispectral cameras and the non-visible part of the spectrum in general have not been explored for remote sensing detection of plastics residues on agricultural soils. RGB cameras further decrease the complexity of data collection and analysis, as additional data processing such as radiometric calibration, which can be more or less challenging depending on light conditions, are not required. Moreover, RGB cameras increase spatial resolution at the cost of spectral resolution. This allows to acquire data with higher ground sampling distance at the same flight height, or to fly higher and cover larger areas in shorter times to acquire data with the same ground sampling distance. The use of RGB cameras, coupled with deep learning, has been shown to result in reasonable plastic film residues mapping on cropland, but it has been limited to the detection of transparent film residues on cotton fields (Zhai et al., 2022; Qiu et al., 2022; Yang et al., 2024). Different film and soil types may require seeing beyond the visible.

Our work aimed at a comprehensive assessment of UAV optical remote sensing use to detect different plastic film residues on cropland. We combined hyperspectral and multispectral proximal sensing with multispectral remote sensing to (i) build spectral libraries for the most common plastic films used in agriculture; (ii) define spectral changes occurring when moving from pristine plastic film to residue in soil; (iii) define possible workflows and sensors for detecting different plastic film residues using UAV technology.

2. Methods

2.1 Proximal sensing

2.1.1 Experimental site and measuring devices

Outdoor measurements of plastic film reflectance were carried out on a rooftop in Louvain-la-Neuve, Belgium, between 10:00 and 18:00 on 24 July 2022, with almost clear sky conditions. The measurements were performed through the parallel use of a spectroradiometer (ASD fieldspec 3; Fig. 1a; Malvern Panalytical, Ltd.), operated via an acquisition software in reflectance mode (RS^3; Malvern Panalytical, Ltd.), and a multispectral camera (Micasense RedEdge-MX RX02; Fig. 1b; AgEagle Aerial Systems, Inc.), using a setup similar to Crucil et al. (2019).

The spectroradiometer was used with a fiberoptic cable mounted on a pistol grip (Fig. 1a) to acquire hyperspectral data with 3 nm spectral resolution in the 350–1000 nm region, and 10 nm spectral resolution in the 1000–2500 nm region. The software automatically performed the conversion to reflectance measurements and output data at a 1 nm interval. A Spectralon panel with 12.7x12.7 cm^2 of reflective area (Fig. 1a), provided by the same company manufacturing the spectroradiometer, was used as a white reference to optimize and calibrate the instrument about every 4 minutes, and all the spectra were obtained from the average of 75 spectra, each with 34 ms of integration time. Thus, around 2.5 seconds were needed to perform each measurement. The fiberoptic tip was placed 11 cm above the targets at the nadir position, providing a shadow-free conical field of view with a diameter of 4.9 cm.

The multispectral camera used five imaging sensors to acquire spectral data centred at 475, 560, 668, 717, 842 nm wavelengths — namely blue, green, red, red edge, and NIR (near infrared) bands — with bandwidths of 32, 27, 16, 12, 57 nm, respectively. Images of a reflectance panel were acquired before every measurement and used to calibrate and convert data to reflectance values in a later stage. The reflectance panel used had the following reflectance values for RedEdge-MX cameras with serial numbers RX02: blue = 47.49 %; green = 47.73 %; red = 47.81 %; red edge = 47.82 %; near infrared = 47.72 %. The camera was placed 70 cm above the targets at the nadir position, providing around 0.5 mm/pixel images.

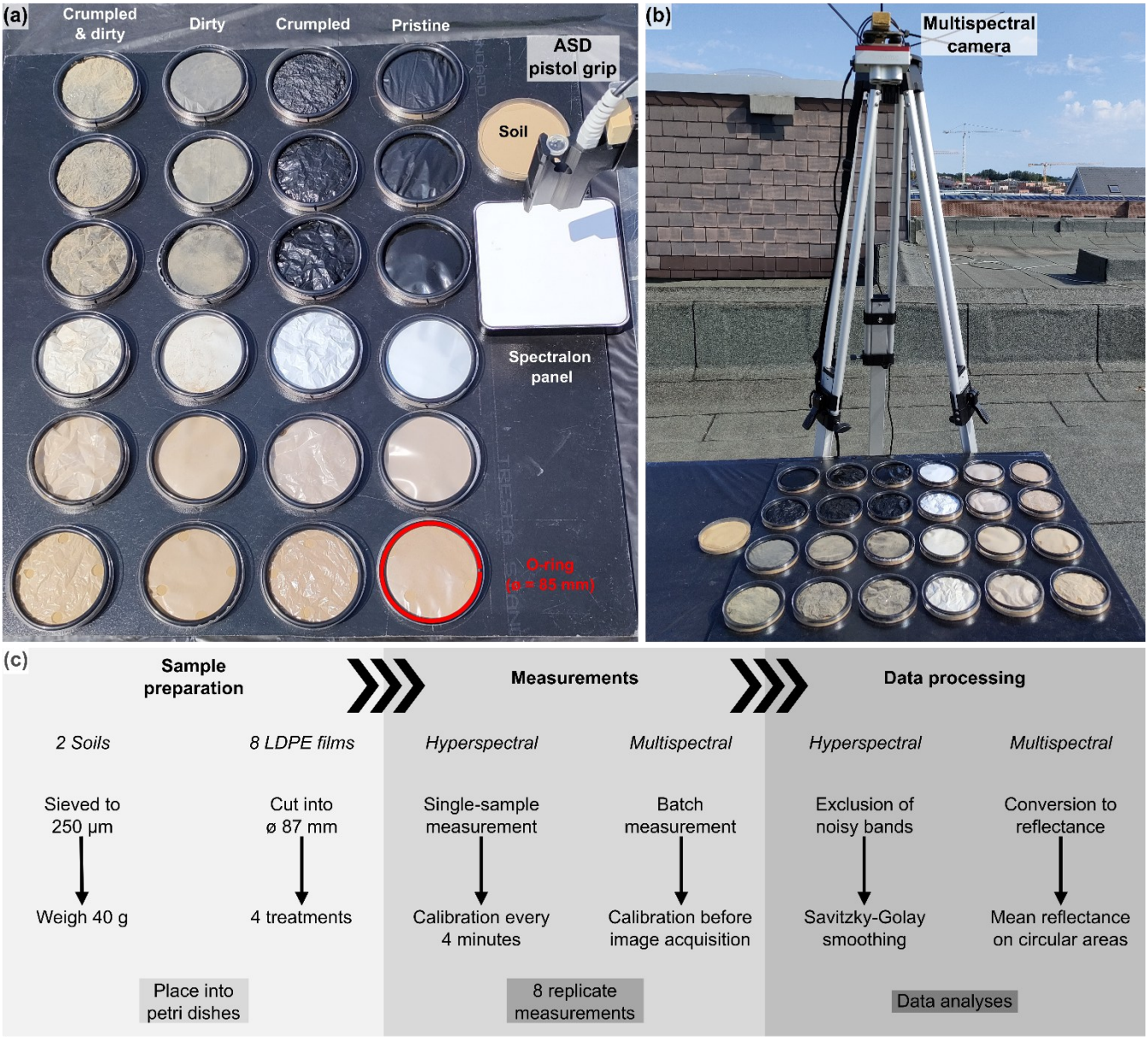

Figure 1 – Experimental setup used for acquiring reflectance measurements of plastic films from a spectroradiometer (i.e., ASD) (a) and a multispectral camera (b), and workflow used (c). The same batch of samples is represented on the left (a) and on the right part of the image (b). On the left side (a), columns were labelled according to the treatment; different rows show different film types, from top to bottom: Black - biodegradable, Black - type 1, Black&White - small (black side), Black&White - small (white side), Transparent - large, Transparent - with holes. Film names refer to Table 1.

2.1.2 Plastic films, soil backgrounds, and experimental workflow

The measurements were performed on eight different LDPE films (Table 1), where double-sided black and white films were used on both sides and virtually increased the number of films to 10. Each plastic film was analysed in four different conditions: pristine, crumpled, dirty, and crumpled and dirty. Crumpling was obtained by manually rubbing the films to obtain a homogenous and randomized crease pattern (Fig. 1a), while dirtiness was obtained by rolling the films into a dry soil volume, thus creating a layer of soil particles attached to the film (Fig. 1a). A field soil (i.e., directly collected from a site), coming from arable land in the Belgian loam belt, where soils are characterized by organic carbon content of 1.26 ± 0.37 % C and classified as silt loam according to USDA classification (Zhang et al., 2021), and a standard soil (LUFA 2.2), characterized by organic carbon content of 1.72 ± 0.54 % C and classified as sandy loam according to USDA classification, were used for the experiment. The two soils were used to make the films dirty and as backgrounds for the measurements on plastic films. Both soils were sieved down to 250 µm, to remove coarser organic and inorganic matter, enabling the acquisition of stable soil spectra and ensuring that pristine films surface would not be influenced by soil roughness. Around 40 g of soil were placed into 87 mm petri dishes. The plastic films were cut to fit into the petri dishes, then the four treatments were applied, and finally, the films were placed on the soil surface in the petri dishes (Fig. 1). Additionally, some petri dishes were left with soil only and used as a reference spectrum of the soil backgrounds (Fig. 1). The use of black nitrile rubber O-rings (Fig. 1) with 85 mm of outer diameter and 75 mm of inner diameter was necessary to fix the films in the petri dishes and prevent wind from blowing them away.

The measurements were performed on a table covered with a black plastic film, and the samples were placed on a black painted wood board (Fig. 1) to minimise background reflectance. However, background measurements were not performed. The petri dishes and the board were marked to allow for positioning the samples always at the same angle, minimising the influence of sample displacement on optical phenomena. The measurements were carried out in batches of a maximum of 25 samples (Fig. 1). First, hyperspectral measurements were performed on individual samples (Fig. 1a). At the end of the batch, one multispectral image was acquired over all the samples in the batch (Fig. 1b) Overall, 82 samples were analysed, i.e., (10 films x 4 treatments x 2 soil backgrounds) + 2 soils. For each sample, five replicate measurements were carried out throughout the day.

Table 1 - Specifications of the LDPE plastic films used for the experiment. Thickness was obtained from the average of 10 measurements performed with a micrometer.

Name	Thickness (µm)	Application mode	Common use	Duration use	Colour
Black - type 1	18 ± 2	On the soil surface	vegetables or fruits	one growing season	black
Black - type 2	18 ± 1				
Black - biodegradable	15 ± 2				
Black&White - small (black side) Black&White - small (white side)	99 ± 3		asparagus	multiple growing seasons	black/white
Black&White - large (black side) Black&White - large (white side)	143 ± 5				
Transparent - with holes	44 ± 2		vegetables or fruits		transparent
Transparent - small	157 ± 1	large tunnel film for greenhouses			
Transparent - large	185 ± 6				

2.1.3 Data processing and analysis

Hyperspectral data were processed in R through the package prospectr (Stevens and Ramirez-Lopez, 2025). First, data at wavelengths below 400 nm and above 2400 nm were removed because of excessive noise in the outdoor measurements (Crucil et al., 2019; Crucil and Van Oost, 2021). Then, a Savitzky-Golay smoothing (Savitzky and Golay, 1964) was applied with a second order polynomial fit and a window size of 11 nm to remove random noise that can arise from outdoor measurements. Finally, water vapour absorption regions, between 1350 and 1450 nm and between 1800 and 1950 nm, were removed. Two spectra, corresponding to one replicate of pristine Black&White - small (black side) on sandy loam and one replicate of pristine Black&White - large (black side) on sandy loam (Table 1), were removed by visual assessment because of excessive noise (Supplement 1), probably due to rapidly changing light conditions.

The multispectral images were pre-processed for radiometric referencing, vignetting correction, black level compensation and conversion to reflectance, following the procedure given by the original manufacturer (Micasense) and using the script provided by Crucil (2021). Following, mean reflectance values were extracted over circular areas of around 5 cm in diameter, centred in each petri dish. This was done to relate the reflectance of an imaging sensor to a non-imaging sensor having a field of view with 4.9 cm of diameter.

Mean values and standard deviation of the five replicates were calculated for each sample (i) and for each wavelength (λ) to account for variability in plastic film reflectance under changing light conditions. Mean spectra are presented for pristine films only. After calculating the average mean ($\bar{\mu}_i$) and the average standard deviation ($\bar{\sigma}_i$) over the whole spectrum, the following coefficient of variation (CV) was used to describe the variation of measurements between replicates of the same sample:

$$CV_i = \frac{\bar{\sigma}_i}{\bar{\mu}_i} \quad (1)$$

To compare the variability across specific groups of film colours and treatments, further aggregated means of the coefficient of variation were also calculated.

To further compare the treatments, the difference in mean reflectance ($\bar{\rho}$) between the pristine and the treated film were calculated. For each treatment and for each wavelength, the difference (Δ_ρ) is expressed as:

$$\Delta_{\rho_{treatment,\lambda}} = \bar{\rho}_{pristine,\lambda} - \bar{\rho}_{treatment,\lambda} \quad (2)$$

As similarities between spectra of the same film colour groups were observed, Δ_ρ were aggregated for black, white, and transparent films through mean values.

Lastly, the following three plastic indexes were calculated for hyperspectral data only, according to their original equations:

$$HI\_1215 = (1216 - 1197)\frac{\rho_{1235} - \rho_{1197}}{1235 - 1197} + \rho_{1197} - \rho_{1216} \quad \text{(Garaba and Dierssen, 2018)}$$

$$HI\_1732 = (1729 - 1705)\frac{\rho_{1741} - \rho_{1705}}{1741 - 1705} + \rho_{1705} - \rho_{1729} \quad \text{(Kühn et al., 2004)}$$

$$ND\_1715 = \frac{\bar{\rho}_{1590to1630} - \bar{\rho}_{1695to1735}}{\bar{\rho}_{1590to1630} + \bar{\rho}_{1695to1735}} \quad \text{(Castagna et al., 2023)}$$

Where ρ_x is the reflectance at the wavelength x, and $\bar{\rho}_{x\ to\ y}$ is the average reflectance from wavelength x to wavelength y. HI (hydrocarbon indexes) are narrow-band indexes involving three bands, where the middle band represents the wavelength at the absorption feature, and the other two are approximately located before and

after the absorption region. ND_1715 captures the same absorption region represented by HI_1732, but it is a broadband index calculated through a normalised difference between the reflectance before the absorption region and the reflectance at the absorption region. ND_1715 was calculated to assess better the potential of a multispectral imaging sensor on a moving platform, which may require broader bandwidths to increase signal-to-noise ratio. To differentiate index values of plastic films from other possible targets (i.e. soil and crop residues), we have extracted index values of soils and crop residues from open spectral libraries (Hively, 2021; Kokaly, 2017).

2.2 Remote sensing

2.2.1 Test site and equipment

An agricultural field located in the province of Córdoba, Spain (37°59'42.30" N, 4°27'40.41" W) was selected to test UAV capabilities in detecting plastic film residues (Fig. 2). The field is located next to the Guadalquivir River. The typical soil at this location is a calcaric Luvisol soil according to FAO classification (Junta De Andalucía, 2005), with soil organic carbon content of 0.77 ± 0.64 % C (Muñoz-Rojas et al., 2012). Despite management practices not including the use of plastic directly on the field, a few plastic items were found on the field, probably resulting from littering, plastic contamination from neighboring fields, or plastic parts of machines used on the field.

UAV images were acquired with a Phantom 4 pro (SZ DJI Technology Co., Ltd.) equipped with a downwelling light sensor and the same multispectral camera used in the proximal sensing experiment (Micasense RedEdge-MX RX02; Fig. 1b; AgEagle Aerial Systems, Inc.). The images were acquired on 28 September 2022, between 11:30 and 12:00, with clear sky conditions. Images of a reflectance panel were acquired before the flight and used for the radiometric referencing of the images in a later stage. The reflectance panel used had the following reflectance values for RedEdge-MX cameras with serial numbers RX02: blue = 47.49 %; green = 47.73 %; red = 47.81 %; red edge = 47.82 %; near infrared = 47.72 %. The flight height was set to 7 m. The camera used had 1280 x 960 pixels of image resolution, 4.8 cm of sensor width, and 5.4 cm of focal length thus providing images with a spatial resolution of around 0.5 cm/pixel at 7 m of flight height. Additionally, two Reach RS2 RTK GNSS (global navigation satellite system) receivers (Emlid Tech Kft.) were used for placing the plastic films on the field and acquiring their coordinates.

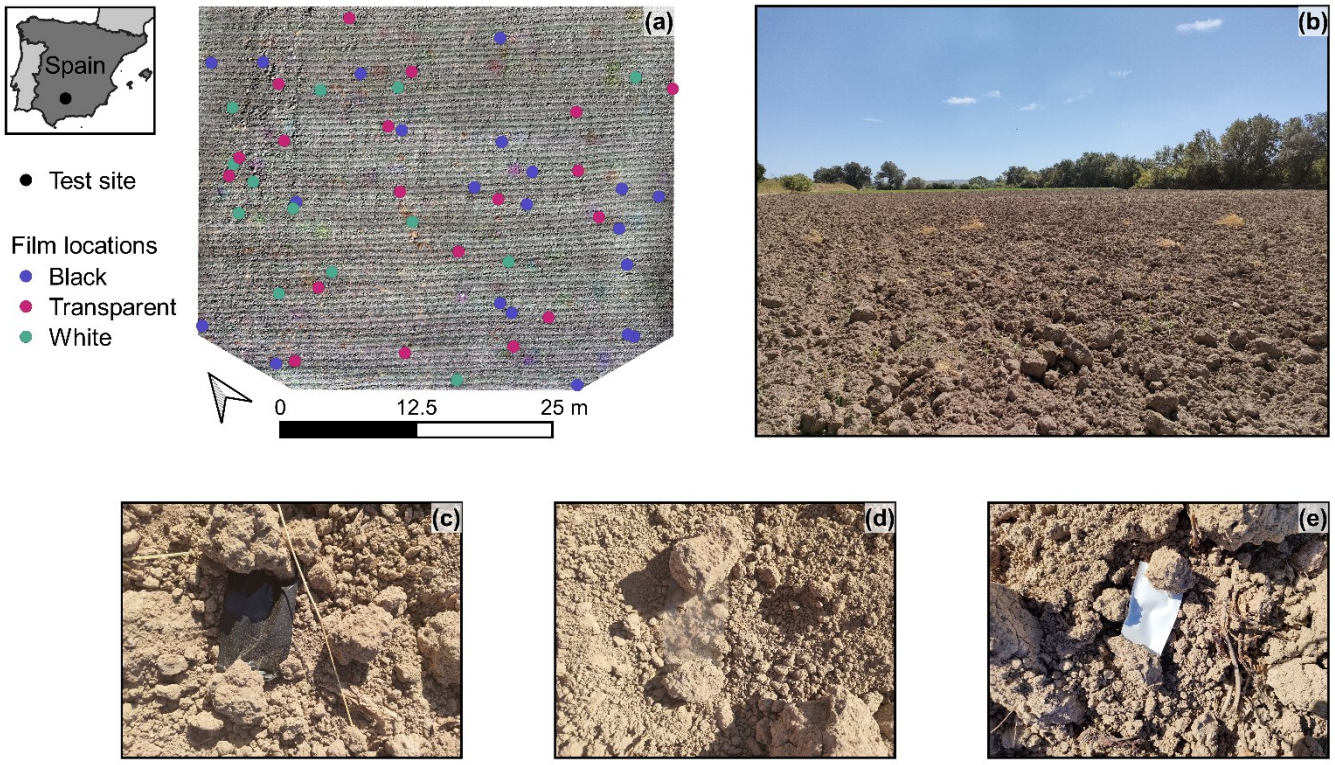

Figure 2 – Location of the study area, distribution of plastic films in the study area (a), field picture (b), and examples of black (c), transparent (d), and white (e) films placed on the field. The geometry of the study area was chosen to maximise the number of plastic films, that are represented by coloured dots (a). On the upper-left corner, the orthomosaic was obtained from the UAV images.

2.2.2 Plastic films and experimental workflow

Three of the films used in the proximal sensing experiment were used for the remote sensing experiment. With reference to Table 1, the plastic films used were: Black - type 1, Black&White - small (white side), and Transparent - with holes. Films were selected to have one black, one white, and one transparent film. The films were cut into 5 cm x 10 cm pieces, and two small holes on the long edges of the films were made to facilitate the penetration of metal spikes that were used to fix the plastic films into the soil. The plastic films were placed on the field using the GNSS receivers, following a random distribution of points previously generated with QGIS (Free Software Foundation, Inc.) (Fig. 2a). After fixing the films into the soil, the metal spikes were covered with soil to avoid their influence on film reflectance. This left a film surface of around 5 cm x 5 cm uncovered and detectable (Fig. 2c–e). In total, 21 black films, 19 transparent films, and 13 white films were placed on the field (Fig. 2a). The experiment was originally designed to place a higher number of films, equally distributed among film colours, on a

larger area. However, it was not possible to acquire images of the entire area, and the study area was restricted to that shown in Fig. 2. This resulted in an uneven distribution of films among the different colours.

2.2.3 Data processing and analysis

Pix4D mapper (Pix4D SA) was used to create orthophoto mosaics through a structure-from-motion algorithm. The same software was used to perform the conversion to reflectance measurements, using data from the downwelling light sensor and the reflectance panel. Reflectance of saturated pixels, acquired as no data by the multispectral camera, was set to the maximum reflectance of 1. The outputs of the pre-processing — five orthophoto mosaics, each representing one of the five bands of the multispectral camera — were used for further analyses in ArcGIS Pro (Environmental Systems Research Institute, Inc.).

The centre of each plastic film was found on the images and labelled according to film colour. Then, 312 random points were generated and labelled by visual interpretation. All the points were labelled as 'soil', and the subclasses 'soil', 'shadow', and 'other' — mainly representing vegetation residues or unidentified classes — were created to allow a better interpretation of the results. Together with the plastic films, these represented the ground observations, which were used for training and testing the classification with a 5-fold cross validation. At each fold, 80 % of the observations is used for training and 20 % of the observations is used for validation. A buffer of 1 cm was applied on training points to increase training features. The buffer was applied after the division between training and validation data, to avoid the selection of validation data within the buffer. The classification was performed through a random forest (Breiman, 2001), with the maximum number of trees set to 50 and the maximum depth of each tree set to 30. After the classification, the images were post-processed using a majority filter on 4-connected pixels, increasing the minimum mapping unit to pixel neighbourhoods but minimizing isolated pixel artifacts. Four different datasets were created to compare the results of different spectral and spatial resolutions:

1. Multispectral 0.5 cm: It contains the original five multispectral bands, plus the following vegetation index: $\text{NDVI (Normalized Difference Vegetation Index)} = \frac{NIR-Red}{NIR+Red}$ (Tucker, 1979)
2. Multispectral 1.2 cm: It contains the same six bands as the multispectral 0.5 cm dataset. The spatial resolution was reduced to 1.2 cm by resampling the raster through nearest neighbour. The resolution was chosen to simulate the resolution obtained from the same multispectral camera at 20 m of flight altitude. This flight altitude is needed to acquire RGB data at 0.5 cm of spatial resolution, following the specifications of the RGB camera mounted on a Phantom 4 Pro.
3. RGB 0.5 cm: It contains the three original visible bands (i.e., red, green, blue).
4. RGB+indexes 0.5 cm: In addition to the three original bands, three band ratios were calculated as follows:

$$\frac{Red}{Green + Blue} \quad (3.1)$$

$$\frac{Green}{Red + Blue} \quad (3.2)$$

$$\frac{Blue}{Red + Green} \quad (3.3)$$

The addition of the band ratios in dataset 4 was done to ensure that at least one RGB dataset had the same number of bands as the multispectral datasets, hence providing the same number of input features into the random forest algorithm.

The detection of the plastic films placed on the field was evaluated against the ground observations by calculating the producer accuracy as the ratio between the number of plastic films correctly detected and the number of plastic films placed on the field. The presence of false positives instead (i.e., pixels classified as plastic but not covered by plastic) was checked by calculating the expected number of pixels covered by plastic, weighted by the producer accuracy, and comparing them with the actual number of pixels classified as plastic. For each film, the expected number plastic covered pixels (N_{pixels}) was calculated as follows:

$$N_{pixels} = N_{films} \times \frac{A_{film}}{A_{pixel}} \times PA \quad (4)$$

Where N_{films} is the number of films placed on the field, A_{film} is the area of a single film, A_{pixel} is the area of a single pixel, and PA is the producer accuracy of the classification.

3. Results

3.1 Spectra of pristine films and plastic indexes

On both soils, the spectra of the films are divided into three groups (Fig. 3): black (Black - type 1, Black - type 2, Black - biodegradable, Black&White - small (black side), Black&White - large (black side)), white (Black&White - small (white side), Black&White - large (white side)), and transparent (Transparent - with holes, Transparent - small, Transparent - large). White and black film reflectance is not particularly influenced by the background soil (Fig. 3). In contrast, transparent film reflectance changes according to the soil, with thinner films being closer to the soil spectra than thicker films (Fig. 3). However, the distance between the plastic film and the soil spectra changes across the spectral region. For instance, Transparent - with holes is closer to the spectra of silt loam in the visible, while Transparent - small gets closer in the NIR and SWIR (Fig. 3). On sandy loam, Transparent - with holes and Transparent - small spectra are very close in the visible, while Transparent - large gets closer to the soil spectra in the NIR and SWIR (Fig. 3). These relationships could be due to different additives in the plastic

films, targeting different uses and influencing the transmittance of the films. Transmittance measurements could further elucidate how plastic film transmittance changes across the spectral region, and could be a relevant topic for crop production (Jones et al., 2021).

Overall, the reflectance of pristine plastic films showed a high coefficient of variation of 40 % on average, while both soils had a similar coefficient of variation of around 4 %. The reflectance of black films is low across the entire spectrum, and the coefficient of variation is 71 % on average, ranging from 10 % for the Black - type 2 on silt loam to 135 % for the Black&White - small (black side) on silt loam. White films have the highest mean reflectance and the lowest coefficient of variation, ranging from 6 % to 17 %. The two different white films present a similar spectral shape, being extremely reflective in the visible spectra, and decreasingly reflective through the SWIR, while the thicker film had higher reflectance across the whole spectra on both soils (Fig. 3). The transparent films generally follow the spectrum of the soil background, and transparent films on a less reflective soil result in lower reflectance of plastic films, and vice versa. The characteristic soil-shaped spectrum is interrupted by absorption features in the SWIR, which are shown by white films at the same wavelengths (Fig. 3). Specifically, the absorption features were found around the following wavelengths: 1215 nm, 1730 nm, 1765 nm, 2312 nm, and 2352 nm. As a result, HI_1215 and HI_1732 allow distinguishing all non-black films, in both pristine and treated conditions, from soils and mixtures, and from crop residues (Fig. 4a,b). While both indices guarantee a complete separability between plastic and non-plastic, HI_1732 values are one order of magnitude greater than HI_1215. ND_1715 has values similar to HI_1732, but the broader spectral interval results in outliers for soils and mixtures, represented by rare minerals (e.g., Erionite, Xenotime) overlaying with ND_1715 values of plastic (Fig. 4c). For both transparent and white films, the indexes generally have higher values for films with a higher thickness (Fig. 4).

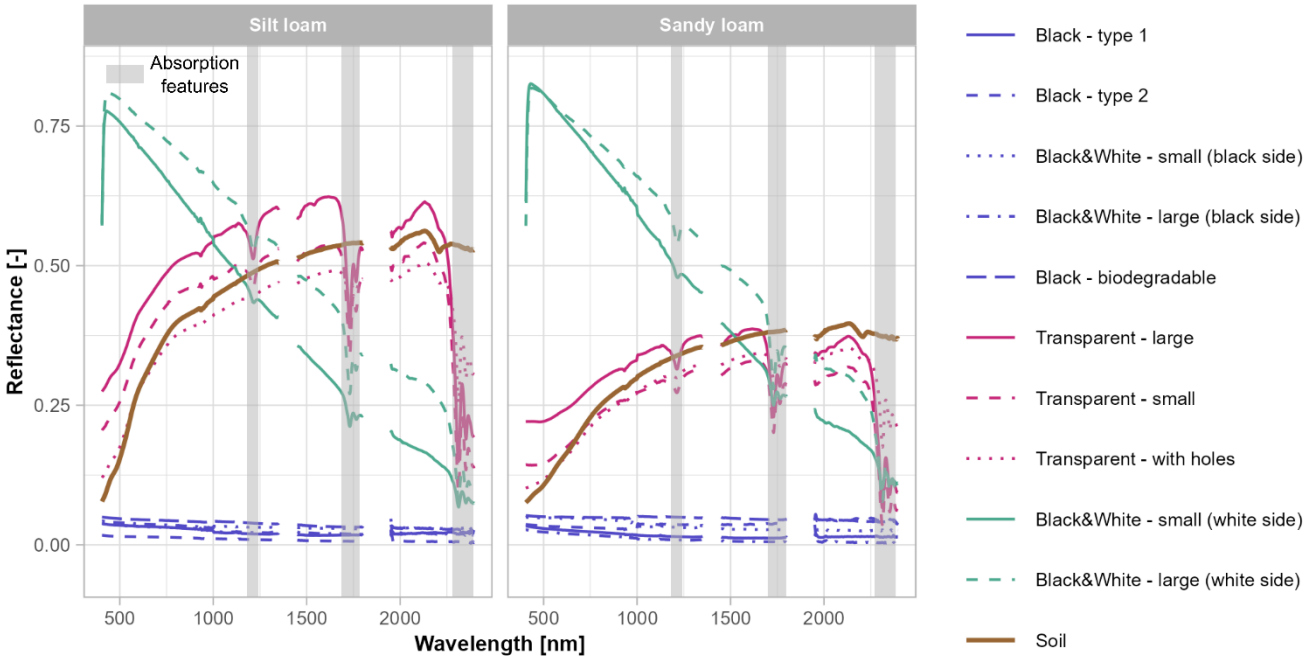

Figure 3 – Spectra of pristine plastic films and of soils used as background. On the left side, spectra acquired on silt loam; on the right side, spectra acquired on sandy loam. Film colours are represented by different colours, and variation within film colours are represented by line shapes. Region of absorption features are highlighted in light grey. Film names refer to Table 1.

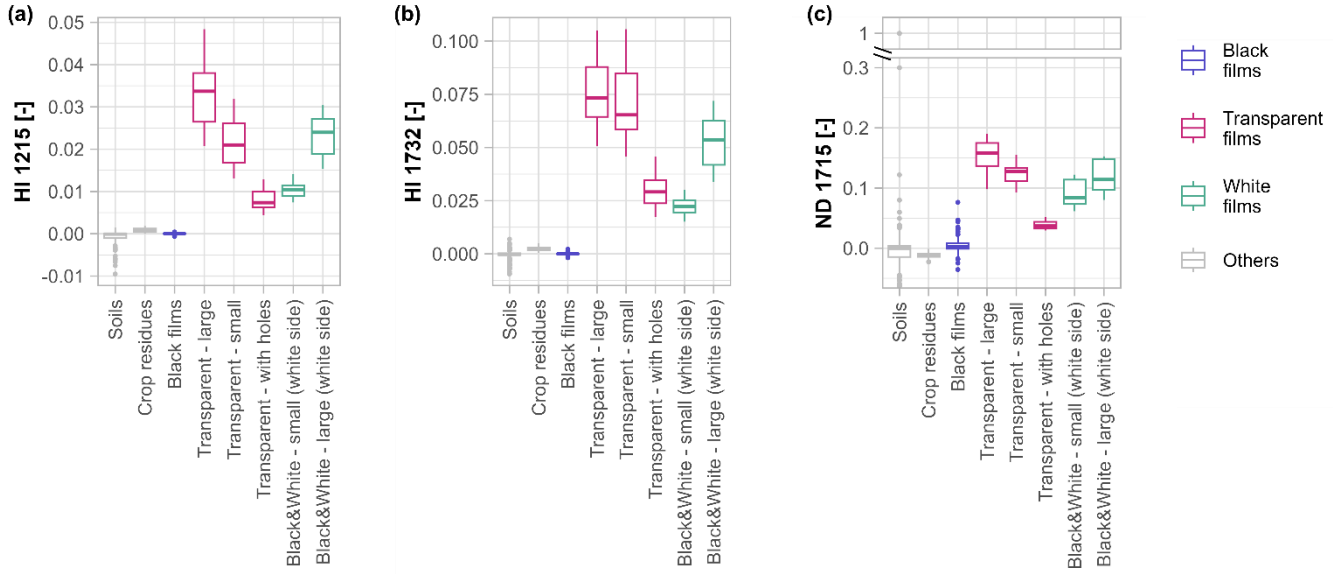

315 **Figure 4 – Boxplots of plastic index values for plastic films, soils, and crop residues. Index values include pristine, crumpled, dirty, and crumpled and dirty films. Values for all black films (i.e., Black - type 1, Black - type 2, Black&White - small (black side), Black&White - large (black side), Black - biodegradable) were aggregated, as they did not represent any relevant value. An axis break was used in (c) to enhance the visualization of the plot.**

3.2 Reflectance of plastic film as residues on soil

320 Compared to pristine films, crumpled and dirty films decreased the reflectance variability between replicate of hyperspectral measurements. The average coefficient of variation was reduced to 30 % for crumpled films, 9 % for crumpled and dirty films, and 9 % for dirty films. Overall, crumpling did not influence plastic film reflectance, as the changes in reflectance are within the range of the coefficient of variation for all the films (Fig. 5, Supplements 2–4). On the contrary, the presence of soil on the film surface influenced plastic film reflectance (Fig. 5, 325 Supplements 2–4). This is particularly evident in the case of white films, where the reflectance of pristine films is substantially higher compared to dirty films in the visible spectra, while the differences between the spectra are reduced for higher wavelengths (Fig. 5, Supplements 2–4). Black film reflectance also changes when covered by soil, but the negative values of reflectance difference in Fig. 5 indicate that the presence of soil increased the reflectance of the plastic films. The differences between spectra increase for higher wavelengths, as soil 330 reflectance increases (Fig. 5). Transparent films are the ones affected the least by treatments, with some changes induced by the presence of soil in the case of sandy loam only (Fig. 5). All these differences were consistently observed for the multispectral measurements in proximal sensing, despite generally higher coefficients of variation (e.g., 45 % for pristine films and 15 % for soils, on average).

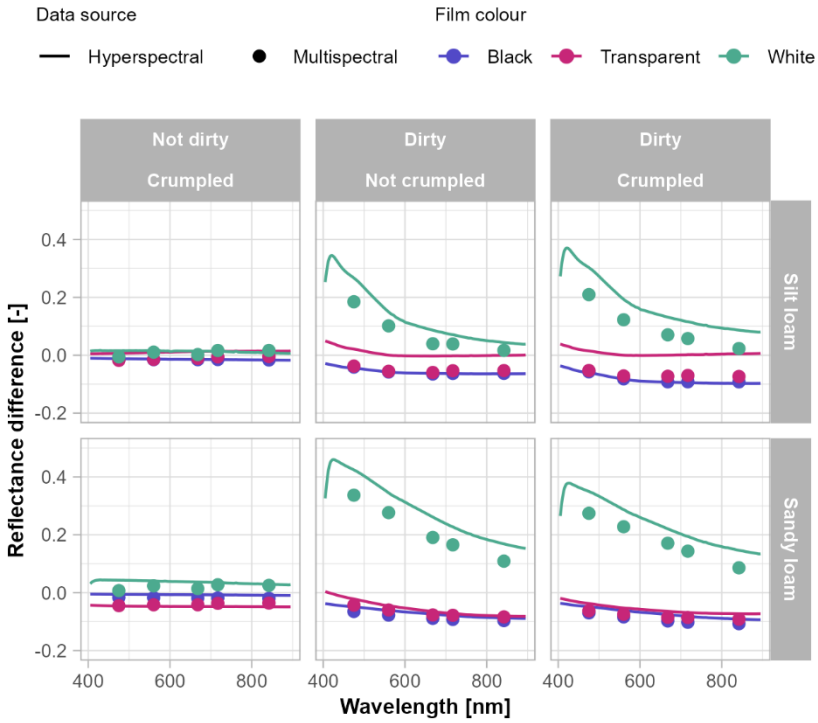

335 **Figure 5 – Mean difference in reflectance between pristine films and treatments, presented for two different soils used as background in the proximal sensing experiment. Different data acquisition modes are represented by shapes, while different film colours are represented by the colour scale.**

3.3 Plastic film detection from UAV

The spectral separability between films and soil observed in proximal sensing is confirmed by the multispectral 340 acquisitions from the UAV (Fig. 6). White films have the highest spectral separability from non-plastic classes, especially in the bands of the visible spectra, while the reflectance slightly overlays with other non-plastic elements when approaching the infrared (Fig. 6). Transparent film reflectance largely overlays with the reflectance of soil and other non-plastic elements, while black films are quite distinct from soils, especially in the infrared bands, where soil reflectance increases (Fig. 6). Overall, all the 0.5 cm datasets had similar 345 performances in detecting the plastic films placed on the field (Fig. 7a), while the multispectral 1.2 cm dataset had higher omission errors. The difference between the 1.2 cm dataset and the 0.5 cm datasets mainly consists in the missed detection of transparent films (Fig. 7a). White films placed on the field were detected with all four datasets in almost every fold, while black films had a generally higher and more fluctuating omission error (Fig. 7a).

Despite the good performances in detecting the plastic films placed on the field, all the datasets overestimated the presence of plastic on the field (Fig. 7b). Overall, plastic overestimation ranges from an average of 21 times for multispectral 1.2 cm dataset to 44 times for RGB 0.5 cm dataset. Black films encountered the highest overestimation compared to the other films, with RGB datasets having a higher overestimation compared to multispectral datasets (Fig. 7b). After black films, transparent films showed the second highest overestimation, finally followed by white films (Fig. 7b). The overestimation was generally related to the confusion of black films with shadows, white films with highly reflective pixels, and transparent films with soil (Fig. 8).

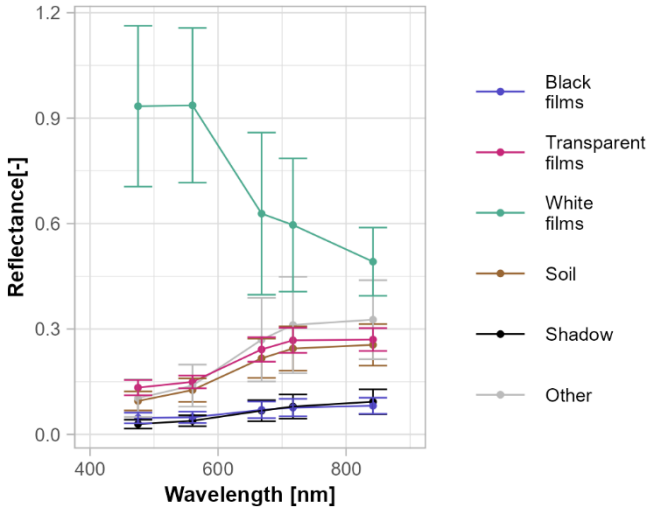

Figure 6 – Reflectance of plastic films divided by colour (i.e., black, transparent, white), compared to soil reflectance, shadow, and other non-plastic objects found on the experimental site.

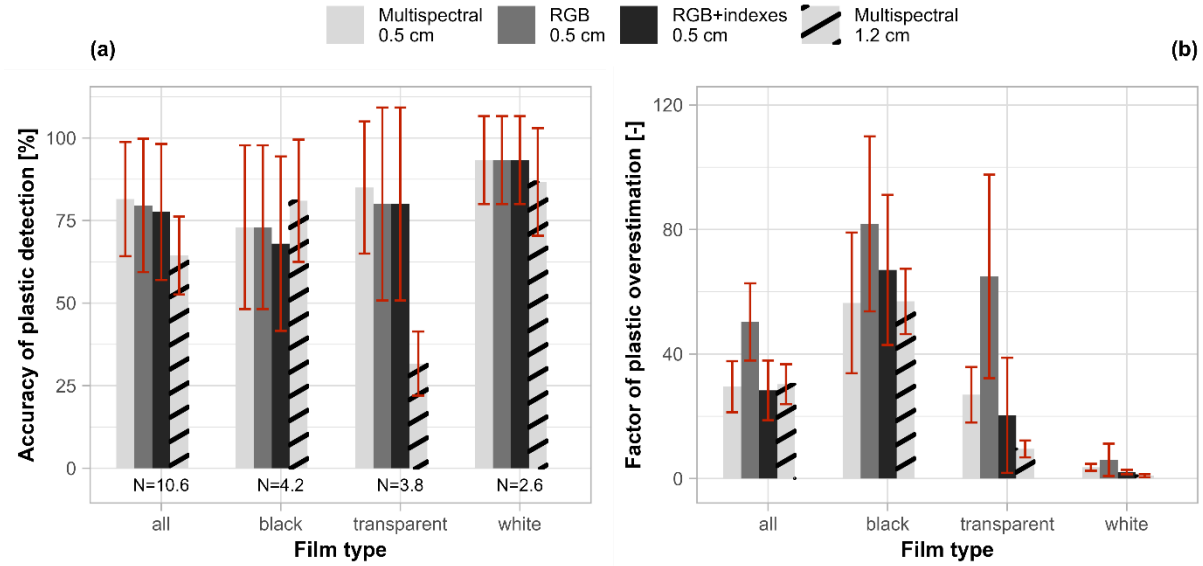

Figure 7 – On the left side, accuracy (i.e., producer accuracy) of plastic detection with four different datasets (a), separated by film and aggregated (i.e., 'all'). Error bars represent the standard deviation of the producer accuracy within the 5-fold cross validation; the numbers below the bars (N) represent the average number of points used for validation. On the right side, factor of plastic overestimation of four different datasets, separated by film and aggregated (b). The factor of plastic overestimation was calculated as the ratio between the detected number and the expected number of plastic-covered pixels. Error bars represent the standard deviation of the overestimation within the 5-fold cross validation.

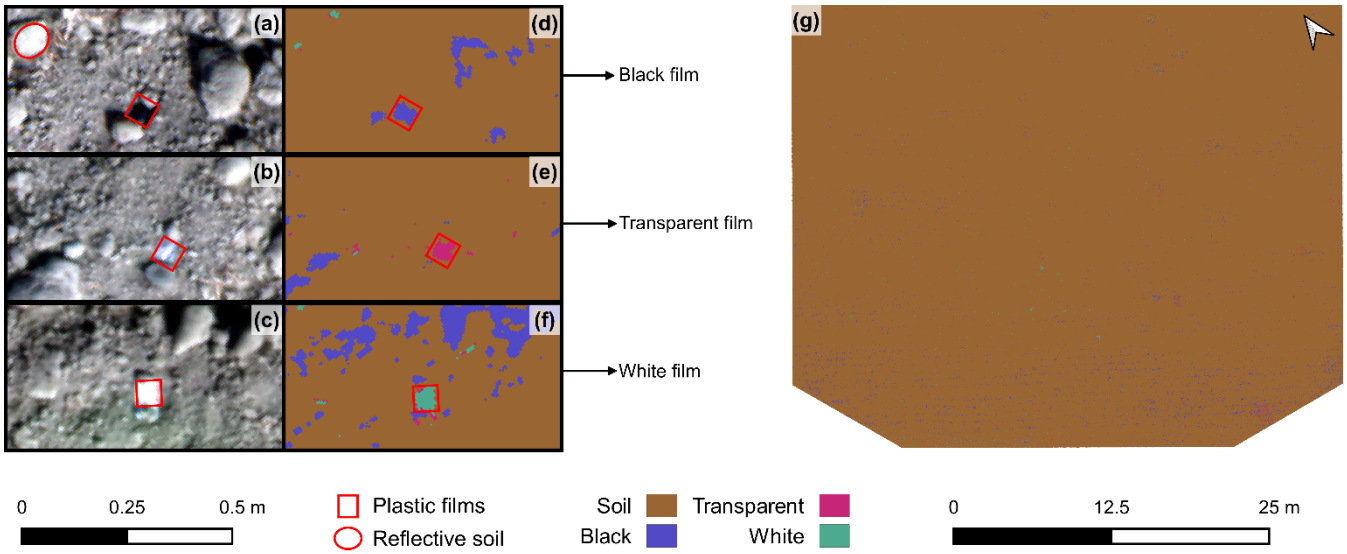

Figure 8 – Detail of the true colour images (a–c) and associated classification results (d–f) obtained with the multispectral 0.5 cm dataset. The classified map is shown in panel (g). On images (a–f), the exact location of the plastic films is highlighted. On image (a), the example of a highly reflective soil region is highlighted.

4. Discussion

4.1 Spectral reflectance of plastic film residues

A spectral library of white, black, and transparent LDPE films was built, nearly covering all plastic film colours used in agriculture. This work introduces an open-access spectral library for agricultural plastic films and explores non-visible regions of the electromagnetic spectrum for identifying plastic films as residues in agricultural soils. Within white and transparent films, differences related to thickness and transparency of the films mainly affected the mean reflectance, while the resulting spectral shapes were highly comparable (Fig. 3). Transparent film spectra are highly influenced by soil spectra (Fig. 3), and our experimental setup allowed to acquire the resulting reflectance of soil and plastic films. An experimental setup such as the one used by Jones et al. (2021) would allow a complete characterization of spectral radiative properties — reflectivity, transmissivity, and absorptivity — and provide insights into spectral changes of transparent films with different backgrounds. Differences between black films can hardly be observed, as spectra are flat and the reflectance is low, producing a low signal-to-noise ratio and high coefficient of variations (Supplement 5).

The mean reflectance of white and transparent films showed much higher variability across replicate measurements compared to soils, resulting in higher coefficients of variation. This is related to both the experimental design and the optical properties of the films. In fact, the measurements were acquired around 4

hours before and 4 hours after solar noon, with solar zenith angle ranging from 32° to 59°, and solar azimuth angle ranging from 103° to 262° (Suncalc.Org). Moreover, the plastic films have a smooth surface, which leads away from the assumption of Lambertian reflector — typically adopted in remote sensing — and causes specular reflection to take over diffuse reflection phenomena (Goddijn-Murphy and Dufaur, 2018; Goddijn-Murphy et al., 2017). This is particularly evident in the case of pristine films, which had the highest coefficient of variation, while the presence of soil on the film surface increases the roughness of the films, favouring diffuse reflection and decreasing the variability of the reflectance between replicates. The implications for plastic residue detection are mostly positive, as particle deposition is expected on land, while specular reflection may be a limiting factor in other applications, such as detection of clean plastic films with satellite data.

Despite a decrease in the coefficient of variation, we did not find any relevant influence of crumpling on film reflectance, while soil was the main driver of changes in reflectance between pristine and treated films (Fig. 5). Changes in plastic film reflectance were particularly evident for white films in the visible spectra, where the distance between the spectra of plastic films and soil is the highest (Fig. 3, Fig. 5). The presence of soil did not have a particular influence on plastic absorption features, enabling plastic identification through spectral indexes, also on soil-covered plastic films (Fig. 4). However, as the amount of soil on the film increases, a progressive deterioration of plastic spectra is expected, until reaching a soil cover at which plastic films will not be detectable anymore. Identifying this threshold of soil cover will be helpful in delineating the boundaries of remote sensing use for detecting plastic film residues on cropland. Our experimental setup did not allow for controlling the amount of soil placed on the films, but aimed at representing field conditions, where soil particle retention of the film surface varies based on film properties. Moreover, indoor spectroscopy would allow exploiting a higher signal-to-noise ratio and better control on the amount of soil placed on the films compared to outdoor measurements, where wind can remove soil particles from the film surface. We also advise against using a contact probe in indoor spectroscopy, as we experienced plastic film surface melting in contact with the light source.

4.2 Use of multispectral and true colour UAV images for plastic film detection

Film spectra acquired from UAV presented similar spectral shapes to the proximal sensing acquisitions (Fig. 3, Fig. 6). White films had very high reflectance for shorter wavelengths and decreasing reflectance for higher wavelengths, transparent films had reflectance similar to soil, and black films had a very low reflectance. However, it must be considered that the reflectance of white films in the UAV acquisitions was highly influenced by assigning the maximum reflectance of 1 to no data values, corresponding to saturated pixels. This particularly influenced the blue and green bands, where the number of saturated pixels was more than half, while the red and red edge bands had around 20 % and 10 % of saturated pixels, respectively, and the NIR had no saturated pixels.

Good performances were achieved in detecting true positives of plastic films (Fig. 7a). Despite the presence of other plastic residues on the field, plastic films were overestimated compared to the expected number of plastic-covered pixels (Fig. 7b). The results of our study might have been influenced by structural flaws of the survey, such as the absence of ground control points or the low overlap of images during flight, which can fall below the recommended threshold of 70 % when flying at 7 m above ground with the camera used. This could have resulted, for example, in band misalignment and halo artifacts that are visible in the RGB composite (Fig. 2a). However, general considerations can be made on how detection accuracy changes depending on the film colour and on the region of the spectrum used.

Specifically, black films had the highest overestimation, which was due to the presence of shadows on the field (Fig. 8a). In our study area, recent tillage practices induced soil clod formation and emphasized the impact of shadows (Fig. 2). However, surface microtopography is always expected on arable land, and we identify shadows as the main limiting factor in black film detection, similarly to previous works dealing with black plastic detection (Iordache et al., 2022; Shan et al., 2018). White films were slightly overestimated in correspondence of highly reflective soil regions (Fig. 8a). As with shadows, the topography of our study area might have emphasized the issue, creating soil surface angles that result in specular reflection and produce high reflectance values, comparable the ones of white films. While techniques like brightness thresholding could improve the results of the classification (Iordache et al., 2022), their implementation and effectiveness may be site-specific, and a few measures could be adopted during data collection to address the challenges related to the illumination geometry. Possible solutions are multi-temporal flights, high-resolution DSM (Digital Surface Model), or flying with a homogenous cloud cover and the highest solar elevation angle possible.

While transparent films had a lower overestimation compared to black films (Fig. 7b), the source of error is related to a strong spectral overlay with soil in the visible and near infrared (Fig. 3, Fig. 6), rather than a structural flaw of the survey. In this case, the only solution to substantially improve plastic detection may be limited to having sensors with bands located in the SWIR. The additional bands on the multispectral camera did not show a substantial improvement in transparent film detection, especially when compared with RGB+indexes 0.5 cm dataset (Fig. 7). For black films, the datasets showed similar producer accuracies, but the multispectral datasets showed a lower overestimation compared to the RGB datasets (Fig. 7). However, the difference in spatial resolution must be considered, as coarser pixel size negatively affects both the areal estimates and the minimum mapping unit. At the same time, for equal pixel size, RGB cameras allow for increasing flight height, consequently reducing flight time and increasing area coverage. Overall, the results of our study suggest that the increased spatial resolution of an RGB camera should be favoured over the higher spectral resolution of multispectral cameras, when aiming at the detection of macroplastic residues of around 5 cm.

Regarding the algorithm used and the experimental setup, it needs to be highlighted that using more sophisticated algorithms like deep learning and image segmentation techniques would likely increase detection

accuracy. However, our experimental setup might have introduced bias when using textural features (e.g., fixed size and shape of plastic films, placement of plastic films under soil clods) and finding the best image classification algorithm goes beyond the scope of our study. Instead, a random forest allowed us to relate the results to spectral features, and to define which sensors and survey workflow are best suited for plastic films detection on soil. Lastly, a high surface occupation of plastic film residues in agricultural fields is rarely documented, and our experiment was designed to replicate a realistic scenario. Future studies could consider increasing the size of the observations related to plastic films to have more robust results.

4.3 A new generation of sensors for monitoring plastic on soil

We have shown potential workflows for detecting plastic film residues with RGB or multispectral cameras. However, the accuracy of these approaches will be site and film specific. A coarse-textured clear soil may represent the optimal site for detecting black films, providing a good contrast between the film and the background, and reducing the complexity of the topography by limiting the formation of soil clods. At the same time, such soils are more likely to induce sensor saturation and a lower contrast with clear films, making the detection of white films harder. On the contrary, a fine-textured dark soil may provide a good environment for white film detection, while black film detection would be limited by a decreased contrast and eventually hindered by the presence of soil clods and direct sunlight. Our study investigated a fraction of all possible soil–plastic film combinations, and further research is needed to comprehensively assess the capabilities of UAV-based detection with current technologies. However, plastics films do not share any absorption feature in the visible and near infrared (Fig. 3), and their identification with currently available multispectral broadband sensors is mostly colour-driven and influenced by spectral shape ambiguities (Garaba, 2025).

While the use of plastic absorption bands in the aquatic environment may be limited by water absorption features (Knaeps et al., 2021; Moshtaghi et al., 2021; Garaba and Dierssen, 2018), their use is extremely promising for soils, with plastic indexes providing an unambiguous identification of the plastic residue (Fig. 4). We showcased the use of plastic indexes available in the literature, but we provided open-access to the spectral library used in this study to promote the development of new spectral indexes and detection algorithms (Garaba, 2025). Within currently available indexes, even the broadband index ND_1715 resulted very effective in identifying plastic films from other elements that could possibly be found on cropland — except for some rare minerals that will not be found on arable land (Fig. 4c) — demonstrating the effectiveness of broad bands located at plastic absorption features and encouraging the development of multispectral cameras tailored to plastic detection. The availability of broad bands related to SWIR absorption features on miniaturised sensors, together with high-resolution visible bands, would reduce costs, data volume, and complexity of currently available hyperspectral sensors, representing a milestone for monitoring any non-black plastic residue on land.

Additionally, according to Castagna et al. (2023), remote sensing offers the potential to distinguish at least three plastic types, exploiting the different locations of absorption features in the SWIR. PE, PP, and PVC — the most produced plastic types in Europe and the most used polymers in agriculture (Plastics Europe Aisbl, 2024) — have similar absorption features, and their distinction might be challenging (Castagna et al., 2023). PET instead — the fourth most produced plastic type in Europe (Plastics Europe Aisbl, 2024) — has different absorption features, and it can be distinguished from PE, PP, and PVC by using narrow-band indexes (Castagna et al., 2023). On agricultural land, this could mean distinguishing plastic residues generated by agricultural management from plastic residues generated by littering (e.g., PET bottles). Building spectral libraries and characterising the absorption features of the most common plastic residues is key to direct future efforts in developing new sensors, which we identify as a necessary technological development to monitor soil plastic contamination. The introduction of legal limits on plastic concentration in soil may not be far off, as initial regulatory examples begin to emerge (Meixner et al., 2020). This will likely drive demand for faster and standardized monitoring and increase the appeal of a sensor for on-soil plastic detection. Moreover, as macroplastic residues can fragment into microplastic (Yang et al., 2022; Song et al., 2017; Julienne et al., 2019), reliable macroplastic monitoring will also support better microplastic assessments.

5. Conclusion

The introduction of miniaturised multispectral imaging sensors has boosted the use of UAV remote sensing. Compared to RGB cameras, multispectral sensors provide access to a few additional bands, typically at the cost of reduced spatial resolution and increased complexity of use. The additional bands available on commercial multispectral sensors are mostly designed for vegetation monitoring, while the detection of plastic residues still relies on the identification of their colour. Within current technologies, our results support using RGB cameras for monitoring plastic film residues on agricultural soils with UAVs, favouring spatial resolution over spectral resolution. However, the accuracy of these techniques will be highly dependent on the type of soil and on the colour of the residue.

The use of plastic absorption features provides an unambiguous identification of the plastic residue, especially on soils. Currently, these features are available only on expensive and complex sensors, hampering their use for monitoring large scales, at which remote sensing is most needed. Plastics are ubiquitous, persistent, and bioaccumulative contaminant that require monitoring plans, and the development of miniaturised sensors targeting plastic detection may represent a pivotal moment for assessing the risk of plastic contamination on land. We expect this work to promote further the exploration of remote sensing potential for monitoring soil plastic contamination and to encourage building and sharing spectral libraries of plastic residues commonly found on soils.

Credit author statement

All authors: writing – review and editing, conceptualization, methodology, resources. **A.F., F.W., P.F.**: visualization. **F.W., P.F**.: supervision, project administration, funding acquisition. **A.F.**: validation, investigation, software, formal analysis, data curation, writing – original draft.

Acknowledgements

This project has received funding from the European Union's Horizon 2020 research and innovation programme under the Marie Skłodowska–Curie grant agreement No 955334. We thank the Institute of Sustainable Agriculture (IAS–CSIC, Córdoba) for the access provided to the research infrastructures. We thank Marco Bravin and Ana Carolina Cugler Moreira for their contribution to the data collection. We thank the members of the Water and Soil Resource Research group of the University of Augsburg for their constant and valuable feedback. Grammarly was used for automated grammar and language proofreading only.

Competing interest

At least one of the (co-)authors is a member of the editorial board of *SOIL*.

Data availability

The spectral libraries used in this research are available at: https://doi.org/10.5281/zenodo.14336253

References

Agriculture Plastic Environment Europe. Statistics - plasticulture in Europe: https://apeeurope.eu/statistics/, last access: 22 December.

Bonifazi, G., Francesconi, E., Gasbarrone, R., Palmieri, R., and Serranti, S.: A preliminary study on the utilization of hyperspectral imaging for the on-soil recognition of plastic waste resulting from agricultural activities, Land, 12, https://doi.org/10.3390/land12101934, 2023.

Breiman, L.: Random forests, Mach. Learn., 45, 5-32, https://doi.org/10.1023/A:1010933404324, 2001.

Castagna, A., Dierssen, H. M., Devriese, L. I., Everaert, G., Knaeps, E., and Sterckx, S.: Evaluation of historic and new detection algorithms for different types of plastics over land and water from hyperspectral data and imagery, Remote Sens. Environ., 298, https://doi.org/10.1016/j.rse.2023.113834, 2023.

Colomina, I. and Molina, P.: Unmanned aerial systems for photogrammetry and remote sensing: a review, ISPRS J. Photogramm. Remote Sens., 92, 79-97, https://doi.org/10.1016/j.isprsjprs.2014.02.013, 2014.

Crucil, G. Application of the radiometric calibration model and image correction: from raw Rededge images to calibrated reflectance: https://github.com/Debrisman/Micasense_Rededge_correction/blob/main/FUN_RededgeM_processing.R, last access: 15 February 2022.

Crucil, G. and Van Oost, K.: Towards mapping of soil crust using multispectral imaging, Sensors, 21, https://doi.org/10.3390/s21051850, 2021.

Crucil, G., Castaldi, F., Aldana-Jague, E., van Wesemael, B., Macdonald, A., and Van Oost, K.: Assessing the performance of UAS-compatible multispectral and hyperspectral sensors for soil organic carbon prediction, Sustainability, 11, https://doi.org/10.3390/su11071889, 2019.

Despini, F., Costanzini, S., Parmeggiani, D., and la Cecilia, D.: Analysis of hyperspectral data to define multispectral sensor specifications for enhancing plastic greenhouse detection, Remote Sens. Appl. Soc. Environ., 101802, https://doi.org/10.1016/j.rsase.2025.101802, 2025.

EIP-AGRI Focus Group: Reducing the plastic footprint of agriculture - final report, European Commission, 2021.

Espí, E., Salmerón, A., Fontecha, A., García, Y., and Real, A. I.: Plastic films for agricultural applications, J. Plast. Film Sheeting, 22, 85-102, https://doi.org/10.1177/8756087906064220, 2006.

FAO: Assessment of agricultural plastics and their sustainability. A call for action, https://doi.org/10.4060/cb7856en, 2021.

Frias, J. P. G. L. and Nash, R.: Microplastics: finding a consensus on the definition, Mar. Pollut. Bull., 138, 145-147, https://doi.org/10.1016/j.marpolbul.2018.11.022, 2019.

Garaba, S. P.: Towards advanced mapping of plastic greenhouses from EMIT, EnMAP and PRISMA hyperspectral missions, Environ. Chall., 22, 101398, https://doi.org/10.1016/j.envc.2025.101398, 2025.

Garaba, S. P. and Dierssen, H. M.: An airborne remote sensing case study of synthetic hydrocarbon detection using short wave infrared absorption features identified from marine-harvested macro- and microplastics, Remote Sens. Environ., 205, 224-235, https://doi.org/10.1016/j.rse.2017.11.023, 2018.

Garaba, S. P., Arias, M., Corradi, P., Harmel, T., de Vries, R., and Lebreton, L.: Concentration, anisotropic and apparent colour effects on optical reflectance properties of virgin and ocean-harvested plastics, J. Hazard. Mater., 406, 124290, https://doi.org/10.1016/j.jhazmat.2020.124290, 2021.

Garaba, S. P., Aitken, J., Slat, B., Dierssen, H. M., Lebreton, L., Zielinski, O., and Reisser, J.: Sensing ocean plastics with an airborne hyperspectral shortwave infrared omager, Environ. Sci. Technol., 52, 11699-11707, https://doi.org/10.1021/acs.est.8b02855, 2018.

Goddijn-Murphy, L. and Dufaur, J.: Proof of concept for a model of light reflectance of plastics floating on natural waters, Mar. Pollut. Bull., 135, 1145-1157, https://doi.org/10.1016/j.marpolbul.2018.08.044, 2018.

Goddijn-Murphy, L., Peters, S., van Sebille, E., James, N. A., and Gibb, S.: Concept for a hyperspectral remote sensing algorithm for floating marine macro plastics, Mar. Pollut. Bull., 126, 255-262, https://doi.org/10.1016/j.marpolbul.2017.11.011, 2017.

Hively, W. D., Lamb, B.T., Daughtry, C.S.T., Quemada, M., Hunt, R. Jr., Serbin, G., Dennison, P.: Reflectance spectra of agricultural field conditions supporting remote-sensing evaluation of non-photosynthetic vegetation cover (ver. 1.1, November 2022), U.S. Geological Survey data release [dataset], https://doi.org/10.5066/P9XK3867, 2021.

Horton, A. A., Walton, A., Spurgeon, D. J., Lahive, E., and Svendsen, C.: Microplastics in freshwater and terrestrial environments: Evaluating the current understanding to identify the knowledge gaps and future research priorities, Sci. Total Environ., 586, 127-141, https://doi.org/10.1016/j.scitotenv.2017.01.190, 2017.

Iordache, M.-D., De Keukelaere, L., Moelans, R., Landuyt, L., Moshtaghi, M., Corradi, P., and Knaeps, E.: Targeting plastics: machine learning applied to litter detection in aerial multispectral images, Remote Sens., 14, https://doi.org/10.3390/rs14225820, 2022.

Jones, H., Black, T. A., Jassal, R. S., Nesic, Z., Johnson, M. S., and Smukler, S.: Characterization of shortwave and longwave properties of several plastic film mulches and their impact on the surface energy balance and soil temperature, Sol. Energy, 214, 457-470, https://doi.org/10.1016/j.solener.2020.11.058, 2021.

Julienne, F., Delorme, N., and Lagarde, F.: From macroplastics to microplastics: role of water in the fragmentation of polyethylene, Chemosphere, 236, 124409, https://doi.org/10.1016/j.chemosphere.2019.124409, 2019.

Junta de Andalucía. Mapa de Suelos de Andalucía: https://portalrediam.cica.es/VisorRediam/?lyr.add.wms=http%3A%2F%2Fwww.juntadeandalucia.es%2Fmedioambiente%2Fmapwms%2FREDIAM_Suelos_Andalucia%3F, last access: 9 April 2025.

Kawecki, D. and Nowack, B.: Polymer-specific modeling of the environmental emissions of seven commodity plastics as macro- and microplastics, Environ. Sci. Technol., 53, 9664-9676, https://doi.org/10.1021/acs.est.9b02900, 2019.

Kedzierski, M., Cirederf-Boulant, D., Palazot, M., Yvin, M., and Bruzaud, S.: Continents of plastics: an estimate of the stock of microplastics in agricultural soils, Sci. Total Environ., 880, 163294, https://doi.org/10.1016/j.scitotenv.2023.163294, 2023.

Knaeps, E., Sterckx, S., Strackx, G., Mijnendonckx, J., Moshtaghi, M., Garaba, S. P., and Meire, D.: Hyperspectral-reflectance dataset of dry, wet and submerged marine litter, Earth Syst. Sci. Data, 13, 713-730, https://doi.org/10.5194/essd-13-713-2021, 2021.

Kokaly, R. F., Clark, R.N., Swayze, G.A., Livo, K.E., Hoefen, T.M., Pearson, N.C., Wise, R.A., Benzel, W.M., Lowers, H.A., Driscoll, R.L., Klein, A.J.: USGS Spectral Library Version 7 Data, U.S. Geological Survey data release [dataset], https://doi.org/10.5066/F7RR1WDJ, 2017.

Kühn, F., Oppermann, K., and Hörig, B.: Hydrocarbon Index – an algorithm for hyperspectral detection of hydrocarbons, Int. J. Remote Sens., 25, 2467-2473, https://doi.org/10.1080/01431160310001642287, 2004.

Lamont, W. J.: Plastic mulches for the production of vegetable crops, in: A guide to the manufacture, performance, and potential of plastics in agriculture, edited by: Orzolek, M. D., Plastic design library, Elsevier, 45-60, https://doi.org/10.1016/b978-0-08-102170-5.00003-8, 2017.

Landrigan, P. J., Raps, H., Cropper, M., Bald, C., Brunner, M., Canonizado, E. M., Charles, D., Chiles, T. C., Donohue, M. J., Enck, J., Fenichel, P., Fleming, L. E., Ferrier-Pages, C., Fordham, R., Gozt, A., Griffin, C., Hahn, M. E., Haryanto, B., Hixson, R., Ianelli, H., James, B. D., Kumar, P., Laborde, A., Law, K. L., Martin, K., Mu, J., Mulders, Y., Mustapha, A., Niu, J., Pahl, S., Park, Y., Pedrotti, M.-L., Pitt, J. A., Ruchirawat, M., Seewoo, B. J., Spring, M., Stegeman, J. J., Suk, W., Symeonides, C., Takada, H., Thompson, R. C., Vicini, A., Wang, Z., Whitman, E., Wirth, D., Wolff, M., Yousuf, A. K., and Dunlop, S.: The Minderoo-Monaco commission on plastics and human health, Ann. Glob. Health, 89, 23, httpsWater research://doi.org/10.5334/aogh.4056, 2023.

Liu, M., Feng, J., Shen, Y., and Zhu, B.: Microplastics effects on soil biota are dependent on their properties: a meta-analysis, Soil Biol. Biochem., 178, 108940, https://doi.org/10.1016/j.soilbio.2023.108940, 2023.

Lofty, J., Muhawenimana, V., Wilson, C. A. M. E., and Ouro, P.: Microplastics removal from a primary settler tank in a wastewater treatment plant and estimations of contamination onto European agricultural land via sewage sludge recycling, Environ. Pollut., 304, 119198, https://doi.org/10.1016/j.envpol.2022.119198, 2022.

Martin, C., Parkes, S., Zhang, Q., Zhang, X., McCabe, M. F., and Duarte, C. M.: Use of unmanned aerial vehicles for efficient beach litter monitoring, Mar. Pollut. Bull., 131, 662-673, https://doi.org/10.1016/j.marpolbul.2018.04.045, 2018.

Meixner, K., Kubiczek, M., and Fritz, I.: Microplastic in soil–current status in Europe with special focus on method tests with Austrian samples, AIMS Environ. Sci., 7, 174–191, https://doi.org/10.3934/environsci.2020011, 2020.

MicaSense. Radiometric calibration model for MicaSense sensors: https://support.micasense.com/hc/en-us/articles/115000351194-Radiometric-Calibration-Model-for-MicaSense-Sensors, last access: 11 April 2025.

Moshtaghi, M., Knaeps, E., Sterckx, S., Garaba, S. P., and Meire, D.: Spectral reflectance of marine macroplastics in the VNIR and SWIR measured in a controlled environment, Sci. Rep., 11, 5436, https://doi.org/10.1038/s41598-021-84867-6, 2021.

Muñoz-Rojas, M., Jordán, A., Zavala, L., De la Rosa, D., Abd-Elmabod, S., and Anaya-Romero, M.: Organic carbon stocks in Mediterranean soil types under different land uses (southern Spain), Solid Earth, 3, 375-386, https://doi.org/10.5194/se-3-375-2012, 2012.

Pahlawan, M. F. R., Kim, Y., Aline, U., Zahroh, A., Masithoh, R. E., Kim, M. S., Baek, I., and Cho, B.-K.: Non-destructive identification of microplastics in soil using spectroscopy and hyperspectral imaging, Trends Anal. Chem., 118216, https://doi.org/10.1016/j.trac.2025.118216, 2025.

Plastics Europe AISBL. The circular economy for plastics - a European analysis: https://plasticseurope.org/wp-content/uploads/2024/03/CEreport_executivesummary_2024.pdf, last access: 11 April 2025.

Qiu, F., Zhai, Z., Li, Y., Yang, J., Wang, H., and Zhang, R.: UAV imaging and deep learning based method for predicting residual film in cotton field plough layer, Front. Plant Sci., 13, 1010474, https://doi.org/10.3389/fpls.2022.1010474, 2022.

Rehm, R., Zeyer, T., Schmidt, A., and Fiener, P.: Soil erosion as transport pathway of microplastic from agriculture soils to aquatic ecosystems, Sci. Total Environ., 795, https://doi.org/10.1016/j.scitotenv.2021.148774, 2021.

Rezaei, M., Abbasi, S., Pourmahmood, H., Oleszczuk, P., Ritsema, C., and Turner, A.: Microplastics in agricultural soils from a semi-arid region and their transport by wind erosion, Environ. Res., 212, https://doi.org/10.1016/j.envres.2022.113213, 2022.

Savitzky, A. and Golay, M. J.: Smoothing and differentiation of data by simplified least squares procedures, Anal. Chem., 36, 1627-1639, https://doi.org/10.1021/ac60214a047, 1964.

Scarascia-Mugnozza, G., Sica, C., and Russo, G.: Plastic materials in European agriculture: actual use and perspectives, J. Agric. Eng., 42, 15-28, https://doi.org/10.4081/jae.2011.3.15, 2011.
Shan, J., Zhao, J., Liu, L., Zhang, Y., Wang, X., and Wu, F.: A novel way to rapidly monitor microplastics in soil by hyperspectral imaging technology and chemometrics, Environ. Pollut., 238, 121-129, https://doi.org/10.1016/j.envpol.2018.03.026, 2018.
Song, Y. K., Hong, S. H., Jang, M., Han, G. M., Jung, S. W., and Shim, W. J.: Combined effects of UV exposure duration and mechanical abrasion on microplastic fragmentation by polymer type, Environ. Sci. Technol., 51, 4368-4376, https://doi.org/10.1021/acs.est.6b06155, 2017.
Steinmetz, Z., Löffler, P., Eichhöfer, S., David, J., Muñoz, K., and Schaumann, G. E.: Are agricultural plastic covers a source of plastic debris in soil? A first screening study, Soil, 8, 31-47, https://doi.org/10.5194/soil-8-31-2022, 2022.
Stevens, A. and Ramirez-Lopez, L. An introduction to the prospectr package: https://cran.r-project.org/web/packages/prospectr/vignettes/prospectr.html, last access: 10 April 2025.
SunCalc.org. https://www.suncalc.org/#/50.6693,4.62,17/2022.07.24/10:00/1/3, last access: 11 April 2025.
Thompson, R. C., Olsen, Y., Mitchell, R. P., Davis, A., Rowland, S. J., John, A. W., McGonigle, D., and Russell, A. E.: Lost at sea: where is all the plastic?, Science, 304, 838, https://doi.org/10.1126/science.1094559, 2004.
Tucker, C. J.: Red and photographic infrared linear combinations for monitoring vegetation, Remote Sens. Environ., 8, 127-150, https://doi.org/10.1016/0034-4257(79)90013-0, 1979.
Veenstra, T. S. and Churnside, J. H.: Airborne sensors for detecting large marine debris at sea, Mar. Pollut. Bull., 65, 63-68, https://doi.org/10.1016/j.marpolbul.2010.11.018, 2012.
Wang, P.-Y., Zhao, Z.-Y., Xiong, X.-B., Wang, N., Zhou, R., Zhang, Z.-M., Ding, F., Hao, M., Wang, S., Ma, Y., Uzamurera, A. G., Xiao, K.-W., Khan, A., Tao, X.-P., Wang, W.-Y., and Tao, H.-Y.: Microplastics affect soil bacterial community assembly more by their shapes rather than the concentrations, Water Res., 245, 120581, https://doi.org/10.1016/j.watres.2023.120581, 2023a.
Wang, Y., Xiang, L., Amelung, W., Elsner, M., Gan, J., Kueppers, S., Christian, L., Jiang, X., Adu-Gyamfi, J., Heng, L., Sik Ok, Y., Ivleva, N. P., Luo, Y., Barceló, D., Schäffer, A., and Wang, F.: Micro-and nanoplastics in soil ecosystems: Analytical methods, fate, and effects, Trends Anal. Chem., 169, 117309, https://doi.org/10.1016/j.trac.2023.117309, 2023b.
Yang, J., Zhai, Z., Li, Y., Duan, H., Cai, F., Lv, J., and Zhang, R.: Design and research of residual film pollution monitoring system based on UAV, Comput. Electron. Agr., 217, https://doi.org/10.1016/j.compag.2023.108608, 2024.
Yang, Y., Li, Z., Yan, C., Chadwick, D., Jones, D. L., Liu, E., Liu, Q., Bai, R., and He, W.: Kinetics of microplastic generation from different types of mulch films in agricultural soil, Sci. Total Environ., 814, 152572, https://doi.org/10.1016/j.scitotenv.2021.152572, 2022.
Zhai, Z., Chen, X., Zhang, R., Qiu, F., Meng, Q., Yang, J., and Wang, H.: Evaluation of residual plastic film pollution in pre-sowing cotton field using UAV imaging and semantic segmentation, Front. Plant Sci., 13, 991191, https://doi.org/10.3389/fpls.2022.991191, 2022.
Zhang, H., Shi, P., Crucil, G., Wesemael, B., Limbourg, Q., and Van Oost, K.: Evaluating the capability of a UAV-borne spectrometer for soil organic carbon mapping in bare croplands, Land Degrad. Dev., 32, 4375-4389, https://doi.org/10.1002/ldr.4043, 2021.
Zhang, J., Ren, S., Xu, W., Liang, C., Li, J., Zhang, H., Li, Y., Liu, X., Jones, D. L., Chadwick, D. R., Zhang, F., and Wang, K.: Effects of plastic residues and microplastics on soil ecosystems: a global meta-analysis, J. Hazard. Mater., 435, https://doi.org/10.1016/j.jhazmat.2022.129065, 2022.
Zhou, S., Kuester, T., Bochow, M., Bohn, N., Brell, M., and Kaufmann, H.: A knowledge-based, validated classifier for the identification of aliphatic and aromatic plastics by WorldView-3 satellite data, Remote Sens. Environ., 264, https://doi.org/10.1016/j.rse.2021.112598, 2021.
Zhou, S., Mou, L., Hua, Y., Zhang, L., Kaufmann, H., and Zhu, X. X.: Can we use deep learning models to identify the functionality of plastics from space?, Int. J. Appl. Earth Obs. Geoinf., 123, https://doi.org/10.1016/j.jag.2023.103491, 2023.